Studying *miR-34a*-mediated gene regulation during hepatic embryogenesis

Madalena Pereira de Freitas [1,2]

Dr Paulina Zydowicz-Machtel [2]

Dr. Tiago Paulo Gonçalves Fernandes [1]

1. Instituto Superior Técnico; Avenida Rovisco Pais, nº1,1049-001 Lisboa
2. Karolinska Institutet, Department of Cellular and Molecular Biology, Emma Andersson Lab, Solnavägen 9, 171 65 Solna Sweden.

Abstract

Millions of cells emerge, differentiate, and die from embryonic development to adulthood. This is controlled by regulatory mechanisms that ensure accurate gene expression. Their failure leads to developmental and post-natal disorders such as liver diseases. Globally, around 2 million deaths result from liver pathogenesis each year. Additionally, several liver developmental illnesses are, to this date, untreated, still, efforts are being made to develop efficient therapeutics to treat them. Subsequently, this study uses miRNAs, regulators of gene expression, to target *Notch2* and *Hnf4α*, genes essential during liver development and pathogenesis. As such, *miR-34a*, a regulator of these two genes, was encapsulated with lipid nanoparticles (LNPs) as a transfection agent and utilised in this study. Seven chemically modified *miR-34a* variants were tested to surpass transfection limitations and determine which modifications lead to more effective regulation of the target genes. This analysis was performed in the E13.5 hepatoblasts to mimic embryonic development, while RT-qPCR measured the downregulation efficiency. With the attained results, 48h was established as the best transfection and downregulation time for the tested *miR-34a*-LNPs. It was also possible to observe that among all the tested modifications of *miR-34a*-LNP, phosphorylation at the 5'-end with one phosphorothioate bond at each molecule's end leads to higher transfection and downregulation efficiencies. Together these results take nucleic acid therapeutics one step further, primarily in battling hepatic developmental and perinatal disorders.

Keywords: liver development, *miR-34a*, LNPs, *Hnf4α*, *Notch2.*

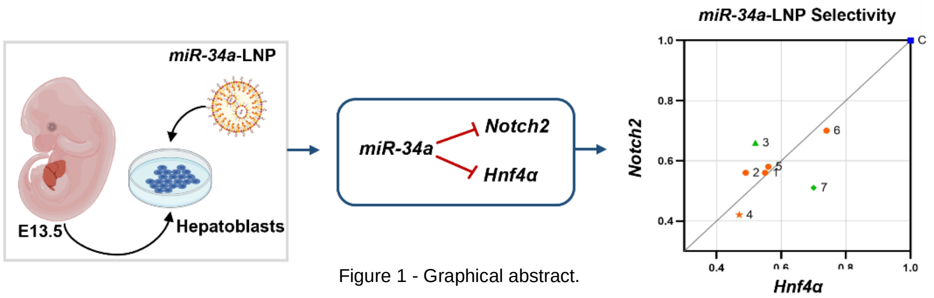

Figure 1 - Graphical abstract.

Introduction

The liver is a pivotal organ composed of multiple cell types, mainly prevenient from the endoderm. In mice, at embryonic day (E) 8.5, the liver progenitor cells, hepatoblasts, start differentiating at the ventral foregut, establishing the beginning of hepatic specification [1]. The hepatoblasts will migrate and differentiate into hepatocytes and cholangiocytes, the two primary hepatic cell types [2]. After hepatic specification, the hepatoblasts initiate liver bud morphogenesis [3]. At E8.5, the epithelium at the gut lumen thickens. The intensified cell proliferation promotes endoderm elongation. As such, from a layer of cuboidal cells at the apical region of the liver diverticulum, the liver bud begins to emerge [3]. Between E9.0 and E9.5, the monolayer of cuboidal cells transitions into a multilayer of pseudostratified hepatoblasts [3]. The nuclei of the hepatoblasts start to migrate from the apical to the basal region of the cell, which will lead to the transition of multiple-layered stratified hepatoblasts into a single-layer pseudostratified hepatoblast [3]. From E9.5, the laminin layer disassembles, and the hepatoblasts delaminate and migrate to the septum transversum mesenchyme [3,4]. Once the liver bud has reached the septum transversum mesenchyme, it divides into four distinct lobes [5]. Morphogenesis must be effectively structured to ensure a fully functional organ.

Hepatocytes are the primary hepatic cell type taking up around 70% of the liver cell population. These cells operate in concert with cholangiocytes which cover 3% of the liver cell population [6]. Hepatocytes arise from hepatoblasts in a series of complex differentiation events between E13.5 and E15.5, with a progressively increased expression of genes involved in hepatocyte functions, including metabolism, transport, and detoxification [7]. Hepatoblast differentiation into cholangiocytes represents a divergence from the default differentiation into hepatocytes [7]. Cholangiocyte specification takes place between E11.5 and E15.5.

However, from E13.5 to E17.5, cell adhesion, migration, and tube morphogenesis genes are upregulated, indicating cholangiocyte differentiation [7].

The bile duct is a complex structure formed by a network of ducts responsible for the bile's transport from the liver to the duodenum. When bile duct morphogenesis is impaired, the embryo suffers from cholestasis, commonly followed by inflammation, fibrosis, and liver malfunction [8]. Bile duct formation is initiated at around E15.5, marked by the lining up of cholangiocytes around the mesenchyme, forming the ductal plate [9]. This structure comprises two asymmetric lumens. Hepatoblasts are located on the parenchymal side, whereas cholangiocytes face the portal side. Once all cells in the primitive ductal structure have acquired biliary characteristics, the mature ducts become symmetric, and the hepatoblasts differentiate into cholangiocytes that cover the bile ducts entirely [9].

Liver parenchyma morphogenesis depends on several signalling pathways, transcription factors and epigenetic modifiers. For instance, microRNAs (miRNAs) are vital regulators during liver embryogenesis and maintain normal hepatic physiological functions. MicroRNAs are small non-coding RNAs that regulate target gene expression [10]. These molecules play crucial roles in cell differentiation, proliferation, and survival [10]. Mutations in the miRNA sequence or the mRNA biding sites often lead to embryonic defects and pathogenesis.

MicroRNA biogenesis is initiated by RNA polymerase II, which first transcribes a large primary transcript named pri-miRNA [11,12]. Afterwards, pri-miRNAs are cleaved into a 70-nucleotide pre-miRNA by the microprocessor protein complex [10,13]. Following this initial maturation, the pre-miRNA is exported from the nucleus to the cytoplasm by exportin 5 and a Ras-related nuclear protein [10,14]. When pre-miRNAs reach the cytoplasm, they are further processed by Dicer into small miRNA duplexes [10]. The miRNA duplex is loaded into the Argonaute protein, which removes the passenger strand and leaves the guide strand, the mature miRNA [10]. The Argonaute protein mediates the assembly of the ribonucleotide complex named RNA-induced silencing complex (RISC) [12,15]. Target genes will be complementary to the miRNA guide strand target. Once the mRNA is recognised, the RISC will promote gene silencing. Overall, there are two distinct silencing mechanisms: translational repression and target mRNA degradation [16,17]. Determining which mechanism occurs depends on the degree of complementarity between the target mRNA and the effector miRNA. Both processes are viable for mRNA repression, differing mainly by the complementary extent and origin organism. Some miRNAs can even modulate the expression of different target genes via both mechanisms [18]. Furthermore, one miRNA can have various target genes. The downregulation efficiency among the distinct target mRNAs depends on variables such as hybridisation thermodynamics, miRNA sequence, mRNA availability and secondary structure [19].

Several miRNAs have essential functions during liver development. For example, *miR-34a* can downregulate genes such as *Hnf4α*, and *Notch2*, which are fundamental during liver development. *Notch2* is the most profusely expressed Notch receptor in mice embryonic livers [20]. When *Notch2* is knocked down in mice, the bile ducts of these animals exhibit irregular shapes and present structural biliary abnormalities. [21]. Additionally, *Notch2* deregulation can lead to several disorders, such as Alagille Syndrome [22] and hepatocarcinogenesis [23]. Likewise, *Hnf4α* plays a pivotal role in proper morphological and functional hepatocyte differentiation. Livers with *Hfn4α* deletion present fewer and oddly shaped hepatocytes, which are loosely associated and lack glycogen. Hence, abnormal expression of *Hnf4α* results in discontinuities within the liver parenchyma [24]. Therefore, it is essential to maintain the correct expression of these genes during hepatic development, either by increasing or decreasing their expression. As such, *miR-34a* could be potentially used as therapeutics to restore expression levels of its target genes when these are deregulated.

LNPs are currently the most advanced system to deliver nucleic acids to the target cells. They have been used to successfully deliver a hepatic-specific tumour suppressor miRNA decreasing hepatocellular carcinoma tumour growth by 50% even after 30 days [25]. The use of LNPs aims to tackle two common disputes, target specificity and endosomal escape [26]. These nanoparticles are frequently formulated with a helper lipid, a PEGylated lipid, an ionisable lipid, and cholesterol [27]. The ionisable lipid is the critical element for effective delivery. Once inside the endosomes, this lipid acquires a positive charge. The positively charged LNP will interact with the negatively charged lipids in the inner leaflet of the endosome. The cationic and anionic lipids will form an ion pair and change their conformation into a cone, forming the non-bilayer structure, such as the inverted hexagonal H_{II} phase. This conformation is not supported in the bilayer structure, leading to membrane disruption and miRNA release [28,29]. However, even after successfully delivering, miRNAs still need to survive in the intracellular environment of the target cell. Therefore, an approach used to reduce these effects is chemically modifying the miRNA molecules.

As such, this work aims to determine the influence that *miR-34a* regulation over *Notch2* and *Hnf4α* has during liver embryogenesis. LNPs composed mainly of an ionisable lipid were exploited to deliver *miR-34a* into the isolated hepatoblasts. The used *miR-34a* formulation endured several chemical modifications to surpass intracellular nuclease degradation. As such, it was possible to determine which modification improved intracellular survival the most and led to a more effective downregulation of the two target genes.

Materials and Methods

Ethical Statement

Animal experiments were performed with the approval of the Regional Animal Research Ethical Board of Stockholm, Sweden. The handling of animals and the collection of embryos was done following the EU's ethical permit 2987-2020. The study was conducted on CD1 mice strain at embryonic day 13.5 (E13.5).

Liver collection and hepatoblast isolation

E13.5 embryos were dissected under the stereomicroscope (Leica) in cold PBS. The resultant liver solution was dissociated for 20 minutes at 37˚C in a liver perfusion medium (Gibco). Then it was digested for an additional 20 minutes at 37˚C using a liver digestion medium (Gibco). After that, a cell strainer was used to drain the cell suspension. Red blood cell lysis buffer (155 nM NH4Cl, 10 nM KHCO3, and 0.1 mM EDTA, pH 7.4) was used to lyse the erythrocytes for 5 minutes. The mixture was then supplemented with hepatocyte differentiation media (5% FBS, 1x L-glutamine, 1x non-essential amino acids in DMEM High Glucose medium). The cells were then counted with Countess II Automated Cell Counter Life Technologies). At E13.5, hepatoblasts highly express DLK1 [30]. As such, magnetic beads covered with antibodies that bind to DLK1-positive cells were used to sort the hepatoblasts via magnetic activation cell sorting. Subsequently, cells were incubated with the blocking antibody Rat Anti-Mouse CD16/CD32 (BD Biosciences, 1:100) for 10 minutes on ice. Immediately after, the cells were incubated for 15 minutes on ice with anti-DLK1-FITC (Nordic Biosite) at 1:40. Then, the samples were washed twice with washing buffer (BSA 0.5% and EDTA 2 mM in PBS). The cells were resuspended in 150 ml of buffer, and 15 µl of anti-FITC microbeads (Miltenyi Biotec) were added to the solution for 15 minutes on ice. The hepatoblasts isolation was then conducted on a magnetic column (Miltenyi Biotec), according to the manufacturer's protocol.

Lipid nanoparticle formulation and *miR-34a* variants

After hepatoblast isolation, cells were ready for seeding and transfection. LNPs were used as transfection agents to deliver the seven chemically modified variants of *miR-34a* (*miR-34a*-LNP). The LNPs were assembled with four components: an ionisable lipid (C12-200), a helper lipid (DSPC), cholesterol, and a PEGylated lipid [31]. Seven *miR-34a* variants with different chemical modifications were tested. The chemical modifications include 5'-end phosphorylation, insertion of a 5'-end vinyl phosphate group at the C1 position and substitution of phosphodiester (PO) bonds with phosphorothioate (PS) bonds at the 5' and 3'-ends of the molecule. The sequences of each variant can be seen in Table 1.

Table 1 - Sequences of each *miR-34a* variant. 5'Phosphorylations are marked in red as "PHOS", the substitution of PO by PS is exemplified in blue as "s", and the addition of a vinyl phosphate group is represented in green as "VINYL-P".

***miRNA34a* variants**	**Sequence**
miR-34a-1	UGGCAGUGUCUUAGCUGGUUGU
miR-34a-2	PHOS-UGGCAGUGUCUUAGCUGGUUGU
miR-34a-3	PHOS-UsGGCAGUGUCUUAGCUGGUUGU
miR-34a-4	PHOS-UsGGCAGUGUCUUAGCUGGUUGsU
miR-34a-5	PHOS-UsGsGCAGUGUCUUAGCUGGUUsGsU
miR-34a-6	PHOS-sUsGsGCAGUGUCUUAGCUGGUUsGsU
miR-34a-7	(VINYLP-U)sGsGCAGUGUCUUAGCUGGUUsGsU
scr *miR-34a*	GUUAGUGAUACGAUGAUAAA

Cell culture and transfection

Hepatoblasts were cultured in the 96 well plates pre-coated with 10 µg/ml of fibronectin (Merck) diluted in PBS and incubated at 37˚C for 30 minutes. Depending on the experiment, hepatoblasts were cultured in either non-differentiation or differentiation growth media. For non-differentiation experiments, the cells were diluted in Tanimizu´s media (10% FBS, 1x ITS-X, 0.1 µM Dexamethasone, 10 nM Nicotinamide, 10 ng/ml HGF, 10 ng/ml EGF in DMEM/F-12, GlutaMAXTM supplement [Sigma-Aldrich]). E13.5 hepatoblasts were seeded with a density of 35000 cells/well. For differentiation experiments, cells were diluted in differentiation media (5% FBS, 2 mM L-glutamine, 1x ITS-X, 0.1 µM Dexamethasone in Helin´s MCDB131 media with glutamine [Thermo Fisher Scientific]) supplemented with 4% Matrigel. The cells were seeded on a sandwiched system with Matrigel at the top and fibronectin at the bottom of the wells. Cells were cultured in standard conditions of 37˚C, 5% CO_2 and 95% humidity for 12h, 24h, 48h (non-differentiating medium), and 72h (differentiating medium). After seeding, the cells were transfected with *miR-34a*. The seven *miR-34a*-LNP variants and one scrambled *miR-34a* transfected with LNP (scr-LNP) variant were delivered into the cells at a final concentration of 100 nM in 100 µl of media per well. Additionally, double-stranded *miR-34a* was transfected into the cells using Lipofectamine (*miR-34a*-lipo) RNAiMAX (Thermo Fisher), according to the manufacturer's protocol. Furthermore, as a negative control, the hepatoblasts were transfected with scrambled *miR-34a* (Thermo Fisher Scientific) using the same transfection reagent (scr-lipo). The final concentration per well was 100 nM *miR-34a*, scrambled control, and 0.1 vol/vol % Lipofectamine RNAiMAX. As a control for *Hnf4α* downregulation, siRNA specific for this gene was equally transfected with Lipofectamine RNAiMAX at a final concentration of 100 nM siRNA in 0.1 vol/vol % RNAiMAX (siRNA-*Hnf4α*-lipo).

RNA isolation and RT-qPCR

Total RNA was isolated with a *miR*vana™ miRNA Isolation kit (Thermo Fisher). RNA purity was achieved using two DNase treatments. Initially, the standard DNA-free™ DNA Removal kit (Thermo Fisher) was utilised. This was followed by a more sensitive DNase treatment, DNase I, Amplification Grade (Thermo Fisher). RNA concentration and purity were then measured with Nanodrop. cDNA synthesis for miRNA was performed using TaqMan™ MicroRNA Reverse Transcription Kit (Applied Biosystems™) and TaqMan probes specifically binding to *sno202*, *sno234* and *miR-34a*. cDNA synthesis for total mRNA was performed with the Maxima First Strand cDNA Synthesis Kit for RT-qPCR (Thermo Fisher Scientific). qPCR for miRNA was conducted with TaqMan™ Universal Master Mix II, no UNG (Applied Biossystems™). While qPCR for mRNA was performed with the Fast SYBR™ Green Master Mix (Applied Biosystems™). All kits were used according to the manufacturer's instructions. Three technical replicates were used for the qPCR reactions. The comparative ΔC_T technique was also used to assess *miR-34a*, *Notch2*, *Hnf4α* and *Sox9* expression. Table 2 lists the sequences of all the primers and probes.

Table 2 - Sequences of the forward and reverse primers used for the miRNA reverse transcription and mRNA/miRNA qPCRs.

Gene	Forward Primer	Reverse Primer
Hnf4α (mouse)	*TGCCTGCCTCAAAGCAT*	*CACTCAGCCCCTTGGCAT*
Notch2 (mouse)	*GAACCGTGTGGAGATGAACGAGAC*	*CAGAGGCTGGGAAAGGATGATAGG*
Sox9 (mouse)	*GGCAAAGTTGATCTGAAGCGAG*	*GGTCGTTGGGTGGCAAGTATT*
B-actin (mouse)	*CCTAGGCACCAGGGTGTGAT*	*CATGTCGTCCCAGTTGGTAA*

SDS-PAGE and Western-blot

The cells were lysed and collected with RIPA Lysis and Extraction Buffer (Thermo Scientific™) with cOmplete™, EDTA-free Protease Inhibitor Cocktail (Roche). For each condition, three wells from the 96-well plate were pooled together in a total of 90 µl of Buffer. The lysates were centrifuged at 14 000xg at 4˚C for 15 minutes. Protein concentration was assessed with the colourimetric Pierce 660-nm Protein Assay kit (Thermo Scientific™), according to the manufacturer's procedure and read on a VersaMAx Microplate reader (Molecular Devices). The samples were separated on a Mini-PROTEAN® TGXTM Precast Gel (BioRad) with the BioRad gel electrophoresis system. Precision Plus Protein Dual Color Standards (Bio-Rad) was used as a protein marker. The membrane was blocked with 5% skim milk prepared in 10 ml 1x Tris-buffered saline solution with 0.1% Tween® 20 Detergent (TBST) buffer (0.1% Tween, 900 ml dH20 with 100 ml of 10X TBS (24 g Tris, 88 g NaCl, 900 ml dH_2O, pH 7.6) for 30min-1h at RT on a rocker. The membrane was then incubated with primary anti-goat *Hnf4α* antibody (Santa Cruz) diluted at 1:600 in TBST to a final volume of 10 ml overnight at 4˚C. Then, the membrane was incubated with the secondary antibody and prepared to a final volume of 10 ml at a dilution of 1:10 000 anti-rabbit HRP in 5% skimmed milk for 1h at RT. The developing solution was prepared by mixing clarity western peroxide reagent and clarity western luminol/enhancer reagent at a 1:1 ratio from the Clarity™ Western ECL Substrate (Bio-Rad) kit. The membrane was placed on the Biorad Gel Doc XR+ Imaging System (Bio-Rad) support. The images were analysed with the ImageLab™ version 6.0.1 software.

Statistical Analysis

All experiments were independently executed in triplicates. The number of biological replicates was chosen according to the available experiments. The data was assessed using the one-tailed Mann-Whitney statistical test. The results were presented as a median with an interquartile range. Results were deemed statistically significant at $P<0.05$.

Results

miR-34a-LNP intracellular perseverance and downregulation over time

Initially, cells were cultured for 12h in a non-differentiation medium to assess transfection and downregulation efficiency within the first few hours. This was performed since *Hnf4α* has a short half-life of 6h [32]. After 12h of culture time, variant 1 had the most outstanding transfection efficiency with a *miR-34a* fold rise of 295.85 (Fig.2A). Variant 1 only contains the *miR-34a* nucleotide sequence, unaltered by chemical modifications. This molecule was therefore anticipated to be more vulnerable to exonuclease degradation. However, this was not the case within the initial 12h. The second most efficient construct was variant 4, with a relative level fold rise of 262.84. This variant has a 5'-PHOS and is protected by exonucleases with PS bonds at the 5' and 3'-ends. In contrast, variant 3 had the lowest efficiency with a mere fold increment of 75.6. This molecule only has one PS bond at the 5'-end. Therefore, a single PS bond at the 5'-end is insufficient to significantly improve transfection efficiency or intracellular survival.
The expression levels of *Notch2* and *Hnf4α* after *miR-34a*-LNP transfection were analysed to assess downregulation efficiency. Regarding, *Notch2* downregulation, variant 6 had the highest downregulation effectiveness (Fig.2B). This variant was designed with three PS bonds at the 5'-end and two and the 3'-end. Within the first 12h, an increased number of PS bonds seems to effectively protect the molecule against degradation, causing an augmented activity. In contrast, variant 3 had a much lower downregulation efficiency which is corroborated by its lower relative expression levels, possibly due to nuclease susceptibility. Furthermore, despite variant 1 having the highest downregulation efficiency, it also had the highest variability between the two replicates. Thus, this variant has an unstable activity within the first 12h. This variability may result from the absence of chemical modifications making the molecule susceptible to degradation. As for *Hnf4α*, the variants exhibited a more consistent regulation between the two biological replicates when compared to *Notch2* (Fig.2C). Variant 4 had the highest downregulation efficiency. In contrast, variant 6 had the lowest efficacy over *Hnf4α*. Thus, after

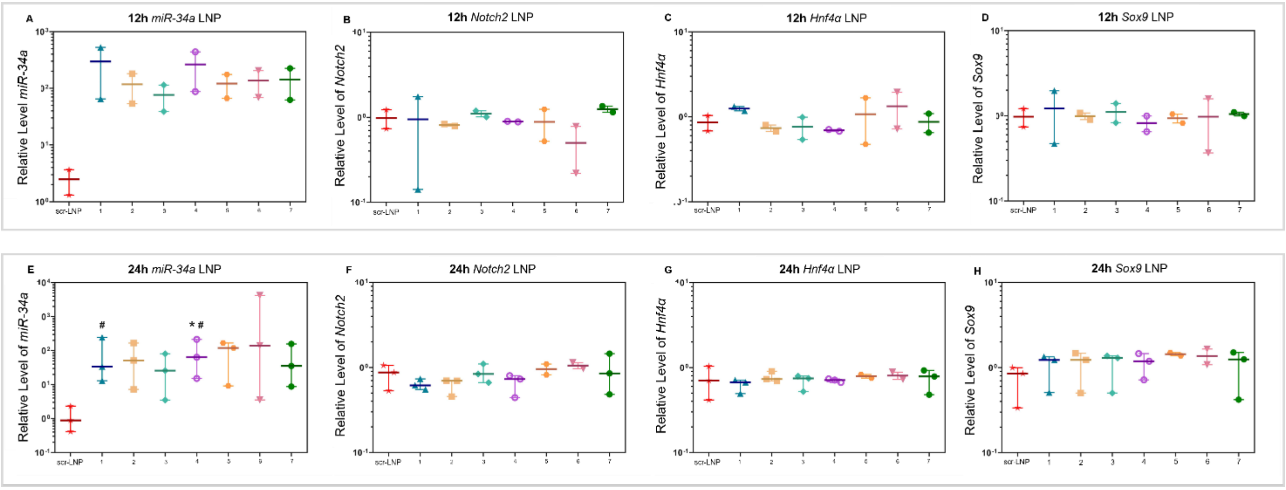

Figure 2 - RT-qPCR after 12 and 24h of *miR-34a*-LNP transfection in isolated E13.5 hepatoblasts. A) *miR-34a* expression after 12h. B) *Notch2* expression after 12h. C) *Hnf4α* expression after 12h. D) *Sox9* expression after 12h. E) *miR-34a* expression after 24h. F) *Notch2* expression after 24h. G) *Hnf4α* expression after 24h. H) *Sox9* expression after 24h. Samples normalised to non-transfected cells set as 1.00. Statistical analysis with Mann-Whitney test, statistically significant results ($p<0.500$) marked as: (*) sample/NT control; (#) sample/scramble control.

12h, this variant demonstrated to be quite selective since it significantly downregulated *Notch2* with a median fold decrease of 0.50 and upregulated *Hnf4α* with a fold increase of 0.33. Moreover, hepatoblasts can either differentiate into hepatocytes or cholangiocytes. The alternative hepatic specification can be distinguished by increased expression of either *Sox9*, a cholangiocyte marker, or *Hnf4α*, a hepatocyte marker. Therefore, it is anticipated that the expression of *Sox9* will increase when *Hnf4α* is downregulated (Fig.2D). However, *Notch2* expression is directly dependent on *Sox9* expression [33]. Thus, the observed upregulation of *Notch2* is expected to result from increased *Sox9* expression levels. As a result of the intercorrelation between *Sox9* and the two target genes, the expression of *Sox9* was also examined 12 hours after *miR-34a* transfection. Transfection of *miR-34a*-LNP, however, showed essentially no impact on *Sox9* levels. This suggests that 12h is not enough time to observe a direct effect of *miR-34a*-LNPs transfection on *Sox9*.

Since 12h of *miR-34a* activity was insufficient to acquire significant and reproducible conclusions, the next step was assessing how the results would change with a longer transfection time. Accordingly, the following experiment was conducted with a 24h time-point in non-differentiating media with three biological replicates. With a relative fold increment of 139.09, variant 6 demonstrated the highest transfection efficiency (Fig.2E). However, it also exhibited the most notable variability among replicates. Analogous to the 12h experiment, variant 3 had a lower transfection efficiency with a median fold rise of 24.72. Additionally, from 12 to 24h of culture, variant 1's transfection effectiveness declined, suggesting that the lack of chemical modifications increased nuclease susceptibility over time. In contrast, after transfection with variant 5, *miR-34a*'s expression level raised over a more extended period. This variant has a 5'-PHOS, and two PS bonds are present at each end, similar to variant 4. Thus, PS bonds at the 5' and 3'-ends seem to increase intracellular persistence.

Target gene downregulation was also assessed after 24h. This time point can be characterised by the high downregulation variability between the *miR-34a*-LNP's biological replicates (Fig.2F). Even though variant 1's intracellular persistence decreased after 24 hours, it downregulated *Notch2* with the most exemplary efficiency, to a median expression level of 0.62. Variants 2 and 4 also led to a considerably *Notch2* downregulation. Variant 6 transfection, despite leading to higher *miR-34a* endogenous levels, had the lowest downregulation efficiency. As such, this is most likely a side effect of the five PS bonds that can reduce the molecule's thermal stability leading to a reduced regulation capacity [34,35]. The downregulation effectiveness of *Hnf4α* among the variant was more consistent throughout the three biological replicates (Fig.2G). However, the downregulation between the variants was strikingly comparable to that seen in the scr-LNP control. Thus, 24h transfection time is not adequate for *miR-34a*-LNP to have an effective downregulation over *Hnf4α*. Concerning *Sox9*, each variant inadvertently increased the expression level of *Sox9* (Fig.2H). Despite being the most successful at downregulating *Notch2* and *Hnf4α*, variant 4 had a minor influence on *Sox9* levels in the transfected cells. In contrast, variant 6 had been the least effective at downregulating the two target genes. However, it led to the highest expression levels of *Sox9*.

In general, after 24h of transfection, the *miR-34a*-LNP downregulation efficiency increased compared to the 12h time. As transfection time increased, variant 1 transfection effectiveness declined. In contrast, the transfection efficiency of variant 5 improved over time. Variant 4 had the best overall downregulation efficiency. All variants, however, showed elevated variance among the three biological replicates. In general, all variants led to increased *Sox9* levels. Surprisingly, *Sox9* had the lowest level increase after variant 4 transfection.

Optimal *miR-34a* activity is reached after 48h

The following experiment was planned with a more extended culture period of 48 hours. This was done to test the hypothesis that a lengthier *miR-34a* activity period would produce more prominent results. To increase the repeatability of the data, four biological duplicates were carried out in a non-differentiating medium under the same circumstances.

After *miR-34a-lipo* transfection, the 48h time-point resulted in the highest *miR-34a* levels (Fig.3A). Variants 1 (p=0.0143), 2 (p=0.0143), 4 (p=0.0143), 5 (p=0.0143), 6 (p=0.0286) and 7 (p=0.0143) led to a statistically significant increase in *miR-34a* levels compared to NT cells. Furthermore, normalised with the scr-LNP, variants 1 (p=0.0286) and 4 (p=0.0143) showed significantly higher levels of *miR-34a*. After 48h, transfection with variant 4 led to the highest relative level of *miR-34a* with a median fold increase of 452.19. In contrast, variant 2 exhibited the least amount of persistence within the cell. With just a 5'-PHOS, this variant resembles the native *miR-34a*. Due to the lack of extra chemical modifications, this molecule may be easily recognised by nucleases. This would result in more rapid decay, accounting for its lower levels after 48h. Likewise, variant 3 also led to low *miR-34a* levels. Regarding *Notch2* downregulation over 48h, all variants substantially downregulated *Notch2* compared to the NT cells (Fig.3B). However, variant 6 did not cause a significant downregulation over *Notch2* compared to the scr-LNP negative control. Variant 4 exhibited, as predicted, the greatest downregulation effectiveness over *Notch2,* decreasing its median expression levels to 0.36. Variant 4's superior efficacy is directly correlated with its higher persistence in the cells after 48h.

By analysing the results from the *miR-34a*-LNP's downregulation efficiency over *Hnf4α*, it is possible to conclude that variants 4 and 2 are the most efficient (Fig.3C). As such, variant 2 effectively downregulated *Hnf4α* despite suboptimal intracellular levels. Therefore, even if variant 2 decays more quickly, the fact that variant 2 resembles *miR-34a* in its normal state may be advantageous since the cell machinery may recognise this molecule more effectively, enabling a faster and more effective downregulation capability. Statistical significance was achieved for variants 2 (p=0.0286) and 4 (p=0.0286). Hence, variants 2 and 4 lead to a statistically significant decrease in *Hnf4α* expression compared to the non-transfected control.

Due to the lack of reproducibility, it is not viable to draw any firm conclusions on the indirect effects of variants on *Sox9* expression levels after 48 hours (Fig.3D). However, a pattern is discernible when *Sox9* relative expression is compared to the downregulation of *miR-34a*'s two target genes. Overall, the downregulation of the two target genes, *Notch2* and *Hnf4α,* leads to a rise in *Sox9* expression. Therefore, this might suggest that *Sox9* expression can increase only to a certain extent. *Sox9* expression levels start to increase less as the downregulation of the target genes, particularly *Notch2* [33], is more accentuated. This was confirmed for variant 4, which drastically downregulated both target genes while slightly affecting *Sox9* expression levels. However, when cells were transfected with variants 1 or 7, there was not a significant decrease in target gene expression, but the expression levels of *Sox9* increased substantially. Therefore, there is no direct effect between *Notch2* and *Hnf4α* downregulation and an increase in *Sox9* expression levels. As a result, an increase in *Sox9* levels is not directly connected with a high downregulation across the two target genes.

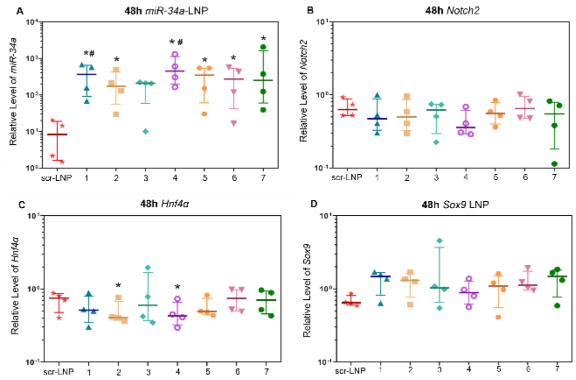

Figure 3 - RT-qPCR after 48h and 24h of *miR-34a*-LNP transfection in isolated E13.5 hepatoblasts. A) *miR-34a* expression. B) *Notch2* expression. C) *Hnf4α* expression. D) *Sox9* expression. Samples normalised to non-transfected cells set as 1.00. Statistical analysis with Mann-Whitney test, statistically significant results (p<0.500) marked as: (*) sample/NT control; (#) sample/scramble control.

Interestingly some variants showed downregulation selectivity over *Notch2* or *Hnf4α.* It is possible to see from Figure 4 that the variants depicted in orange have a similar tendency to downregulate *Notch2* and *Hnf4α*. Furthermore, it is also discernible that variant 4 had the highest downregulation efficiency in the two genes compared to the other variants. Moreover, this downregulation was similar between the two target genes. This infers that one PS bond at 5' and 3'-ends is the optimal level of PS substitution for *miR-34a* activity, intracellular persistence, and transfection efficiency. In contrast, variant 6 had the lowest downregulation efficiency for both genes. This may have been caused by the excess of PS bonds that decreased the molecule's stability and activity [34,35]. Variants 3 and 7 are highlighted in green since they selectively downregulate one gene more than the other. Compared to *Notch2*, Variant 3 appears to downregulate *Hnf4α* more effectively. In contrast, variant 7 preferentially downregulates *Notch2*.

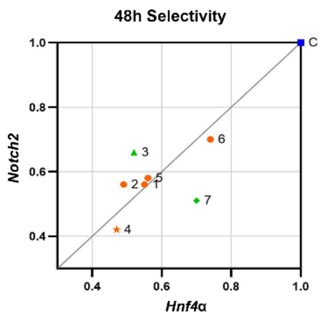

Figure 4 - Downregulation selectivity between *Notch2* and *Hnf4α*. A) MiRs transfected with lipofectamine: *miR-34a* (*miR-34a*-lipo) and siRNA (siRNA-*Hnf4α*-lipo) transfected with RNAiMAX in orange and non-transfected control (C) in blue. B) Samples: scrambled control transfected with LNPs (scr-LNP); *miR-34a* LNP 1, 2, 3, 4, 5, 6,7 transfected with LNPs. Variants with similar downregulation between genes in orange. Variant 3 downregulates more *Hnf4α* (green triangle=. Variant 7 downregulates more *Notch2* (green diamond). Non-transfected control in blue.

***miR-34a*-LNP downregulates *Hnf4α* via translation Repression and mRNA degradation.**

The RT-qPCR results show that some *miR-34a*-LNPs downregulate *Notch2* and *Hnf4α* efficiently. However, miRNAs can downregulate target genes through mRNA degradation or translation repression [16,17]. Therefore, when mRNA is degraded, the levels of mRNA target genes are expected to decrease, as seen in the qPCR results. Nevertheless, after 48 hours of transfection, a Western blot was conducted to measure Hnf4α protein levels to ascertain the mechanism *miR-34a* uses to downregulate *Hnf4α* (Fig.5). For normalisation purposes, B-actin was used as a loading control.
By the western blot results, it is possible to detect a 42kDa band for B-actin and a 52kDa band for Hnf4α. As expected, these bands were brighter for the NT cells, with a dark band. Transfection with scr-lipo slightly decreased the Hnf4α level to 0.60. In contrast, *miR-34a-lipo* and siRNA-*Hnf4α*-lipo decreased Hnf4α protein levels to 0.13 and 0.32, respectively. Variants 6 and 7 had almost no effect on Hnf4α protein levels, as seen by the dark bands displayed on the gel. In contrast, variants 3 and 4 decreased protein levels to 0.38 and 0.44, respectively. Their protein downregulation is similar to that seen in cells treated with siRNA-*Hnf4α*-lipo. The median values for variants 3 and 4 downregulation on mRNA *Hnf4α* were 0.60 and 0.43, respectively. As a result, variant 3's downregulation of *Hnf4α* is more pronounced at the protein level than at the mRNA level. Therefore, it is possible to conclude that variant 3 mainly downregulates *Hnf4α* more via translation inhibition.
Genes with a 3'UTR binding site to *miR-34a* tend to be downregulated via translation inhibition [18]. However, *miR-34a* can regulate the expression of numerous genes by mRNA degradation and translation repression since, for *miR-34a*, the two downregulation mechanisms are co-regulated [18]. More precisely, *miR-34a* can decrease *Hnf4α* mRNA levels in the liver by 40% while decreasing protein expression to 75% [36]. In this work, the preference for *miR-34a* translation repression over *Hnf4α* is evident in the data for variant 3. However, most variants revealed evidence of both downregulation pathways. Hence, it is plausible to conclude that *miR-34a* can reduce hepatic *Hnf4α* levels through mRNA degradation and translation suppression.

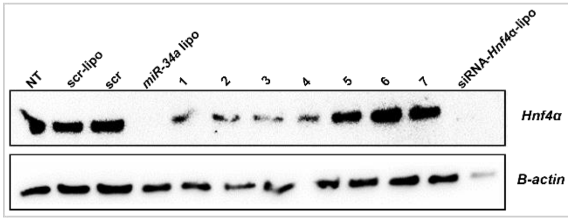

Figure 5 - Western blot analysis of Hnf4α protein after 48h of transfection in E13.5 isolated hepatoblasts. A) Results processed in ImageLabTM version 6.0.1 software.

After 72h, hepatoblasts began to differentiate.

During hepatic embryogenesis, hepatoblasts differentiate into hepatocytes as the default mechanism [7]. Hepatocyte differentiation comes with an increase in the expression of *Hnf4α* [24]. However, hepatoblasts can also differentiate into cholangiocytes exhibited by increased *Sox9* expression [9]. Hence, another question that needs to be answered is whether transfection with *miR-34a*-LNP can modulate hepatoblast differentiation into hepatocyte or cholangiocyte lineage. In case differentiation occurs, it would also be relevant to determine how the *miR-34a*-LNP impacts differentiation. Thus, transfection and downregulation effectiveness were also studied for 72h (Fig.6).
After 72h of transfection, the *miR-34a*-LNPs retained their intracellular persistence. Variant 4 had the highest transfection efficiency with a median fold increase in *miR-34a* levels of 2335.0. Furthermore, all variants transfected with the LNPs retained their activity after 72h. For instance, transfection with variants 2 and 4 had a median fold decreased *Notch2* relative levels of 0.74 and 0.72, respectively (Fig.6A). Only variants 7 and 3 had a negligible impact on the relative expression of *Notch2*. To conclude, even under differentiation, most of the variants successfully downregulated *Notch2*. Regarding the variants' downregulation on *Hnf4α*, the results significantly differed from the pattern observed until this point (Fig.6B). After 72 hours, the downregulation of *miR-34a*-LNP was lower since the variants had a less intense downregulation over this target gene. For instance, variant 4, which had previously had the highest *Hnf4α* downregulation effectiveness, had the lowest effect over *Hnf4α* expression. Thus, it is possible that once differentiation begins, *miR-34a* will highly downregulate *Notch2* while *Hnf4α*'s relative expression starts to increase. However, more experiments would have to be conducted to verify this hypothesis. *Sox9* downregulation after 72h was also assessed. After *miR-34a*-LNP transfection, *Sox9* expression levels were similar to *Notch2*, confirming the inter-dependence between these two genes.

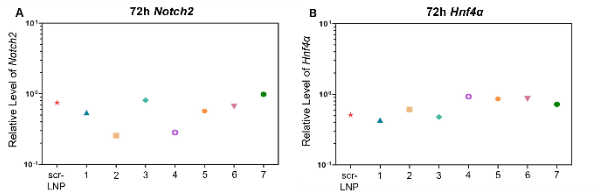

Figure 6 - RT-qPCR after 72h of *miR-34a*-LNP transfection in isolated E13.5 hepatoblasts. A) *Notch2* expression. B) *Hnf4α* expression. Samples normalised to non-transfected cells set as 1.00.

Discussion

Upon *miR-34a*-LNP transfection on hepatoblasts, variants with distinct chemical modifications have different downregulation efficiencies. Therefore, besides establishing that 48h was the optimal time for *miR-34a*-LNP transfection, it was feasible to determine the chemical modifications that resulted in higher miRNA targeted activity. To achieve this, the effectiveness of each variant's downregulation was evaluated separately.

Variant 1 comprises only the naked *miR-34a* sequence. Thus, with time, its intracellular persistence declined. However, this variant displayed a noticeable downregulation efficiency after the first 12 hours. Therefore, when the nuclease exposure time is not prolonged, variant 1 can overcome degradation to a certain extent. One explanation for this transient resistance is that the cell may recognise this variant more quickly after transfection due to the lack of synthetic chemical change. This contradicts most miRNAs since the 5'-end phosphorylation is a determinant factor for miRNA activation [37,38]. After miRNAs are synthesised and phosphorylated, they are loaded into Argonaute and processed into their fully matured form. However, *miR-34a* is an exception to this norm. *miR-34a* activation seems to be dependent on a cellular stress factor. After *miR-34a* synthesis, this molecule can be sequestered in a miRNA intracellular pool. Once the cell receives a stress signal, *miR-34a* is activated by a 5'-end phosphorylation. Only after this process *is miR-34a* loaded to the Argonaute protein to become fully matured [37]. Another hypothesis for variant 1 intracellular survival is that since this variant does not have a 5'-end phosphorylation, it is not active. Its maturation can be hindered, leading to delayed decay. Until now, little is known about miRNA degradation mechanisms. When dephosphorylated *miR-34a* is transfected to the cells, the Argonaute protein does not recognise this molecule, and its full maturation is hampered. Upon synthesis, if miRNA is not loaded in the Argonaute, it cannot undergo enzymatic activities related to decay, such as adding or removing nucleotides known as tailing and trimming, respectively [39]. Furthermore, once matured, miRNAs can have a half-life of up to 24h. Thus, from the time-point at which variant 1 is phosphorylated and becomes active, it can still endure for 24h [39]. All these factors may contribute to the short-time resistance of variant 1.

In contrast, variant 2 had a better transfection and downregulation efficiency throughout the experiments. This variant represents the most natural form of *miR-34a* since it comprises its nucleotide sequence with the activation factor 5'-PHOS [37,38]. The standard effectiveness of this variant may be due to its high similarity to the endogenous *miR-34a*. However, the limited efficiency of this variant may result from the fact that it lacks in extra chemical modifications. Thus, it is an easy target for nuclease degradation. This would explain the quicker decay detected after 48h of transfection. Even so, variant 2 had the second highest downregulation efficiency over *Hnf4α* after 48h. This suggests that the cell may identify this molecule more rapidly, resulting in a more effective downregulation ability.

Compared to variant 2, variant 3 demonstrated a lower transfection and downregulation efficiency. Surprisingly, this molecule has a 5'-PHOS and a PS bond at the 5'-end. It is hence very similar to variant 4. Therefore, it would be anticipated that the outcomes of these two variants would be more comparable. It is, thus, possible to conclude that *miR-34a* is not adequately protected from nuclease degradation by a single PS bond at the 5'-end. The PS bond at the 3'-end is a critical element in intracellular persistence.

With the best-attained transfection rate, variant 4 demonstrated superior downregulation efficacy. This variant has a phosphate group at the 5'-end and one PS bond at the 5' and 3'-ends. The insertion of PS bonds substitutes the non-bridging phosphate oxygen in the phosphate backbone with sulphur, increasing internucleotide linkage resistance to nucleases [40]. As a result, variant 4 is more resistant to exonuclease attacks on both ends, increasing intracellular survival. This increases the *miR-34a* endogenous levels, succumbing to the high downregulation efficiency over both target genes.

Variant 5 is phosphorylated at the 5'-end and contains two PS bonds at each end of the molecule. Thus, this variant differs from variant 4 by the extra PS bond at each end. Overall, this variant also presented ordinary downregulation and transfection efficiency. As a result, the PS bonds at the molecule's 5' and 3'-ends appear to shield it and maintain its intracellular persistence over time. However, an additional PS bond at each end reduced this variant's downregulation effectiveness. Therefore, a single PS bond and each end is the optimal number for transfection and downregulation effectiveness.

Variant 6 had relatively low efficiency and high variability compared to the other variants. For example, variant 6 was the most effective at downregulating this gene at the 12h time-point. In contrast, after 24h, variant 6 had the least downregulation efficiency on *Notch2*. Variant 6 comprises the most PS bonds, with a total of 5 bonds at its ends. Even though PS bonds can protect the molecule against enzyme degradation, PS substitutions can also decrease the thermal stability of the miRNA. For each PS modification, the melting temperature is expected to fall from 0.5 to 0.7°C. [34,35]. Thus, five PS bonds impair *miR-34a*'s stability, decreasing its downregulation activity. Moreover, this variant simultaneously had the highest downregulation efficiency over *Notch2* after 12h and the lowest downregulation efficiency over *Hnf4α*. Thus, at the 12h mark, this variant exhibited a high selectivity among the target genes.

Variant 7 has a 5'-end vinyl phosphate group which is expected to increase intracellular resistance and activity effectiveness. However, this variant presented average results. The 5'-end vinyl phosphate group restricts the group's torsion angle to 180°. Thus, this modification is expected to increase the affinity between the *miR-34a* and the Argonaute protein [41]. Furthermore, the 5'-end vinyl phosphonate group can increase resistance to phosphatases surpassing the 5'-end phosphate predisposition to dephosphorylation [42]. However, this study did not verify the expected effectiveness of this chemical modification.

Additionally, the studied *miR-34a* variants presented downregulation selectivity between *Notch2* and *Hnf4α*. As such, Variant 3 tends to downregulate *Hnf4α* more efficiently than *Notch2*. In contrast, variant 7 preferentially downregulates *Notch2* more than *Hnf4α*. MiRNAs frequently have varied levels of downregulation effectiveness for various target genes. The effectiveness of seed pairing is one of many elements that affect their activity [43]. Both miRNA and the 3' UTR region of the mRNA need to be accessible for interaction. Furthermore, miRNA-mRNA duplexes with lower Gibbs free energy are more stable, resulting in more efficient interactions [43]. However, determining why there is downregulation selectivity in variants 3 and 7 is quite challenging. Variant 3 has a 5'-PHOS with one PS at the 5'-end, differing from variant 7, which comprises a 5'-end vinyl phosphonate group with 2 PS bonds on both sides. As such, this selectivity could be explainable either from the 5'-end or the backbone modification. The vinyl phosphonate group has two main functions that theoretically lead to higher activity. It can protect a miRNA against phosphatases. Furthermore, once the Argonaute protein detects the 5' vinyl phosphate modification, it can adjust its essential residues in the binding pocket to better interact with the miRNA. This enhances the interaction and leads to an improved silencing effect [44]. Still, increased downregulation was not observed in the attained results. Structurally, the vinyl phosphonate group is similar to the phosphate group, thus that they should be equally accessible for mRNA target site binding [45]. The only factor that may change the structure of these two variants is the different number of PS bonds. A PS bond can increase the distance between two adjacent nucleotides [46]. Thus, variant 7 can be more elongated than variant 3. However, variant 5 also has 4 PS bonds and did not exhibit downregulation selectivity. Therefore, neither the 5'-end nor the backbone modification clearly explains the observed selectivity. As such, more experiments would have to be conducted to explain this selectivity.

Furthermore, the isolated hepatoblasts started the hepatic specification process 72 hours after *miR-34a* transfection. In terms of *Sox9*, its expression followed a pattern after *miR-34*-LNP transfection. *Sox9* expression has the propensity to rise when both target genes are downregulated. However, *Sox9* levels do not rise as much when this downregulation is strongly enhanced, as in variant 4. Within its transcription start site, *Notch2* has two binding sites for *Sox9* [33]. As a result, the expression levels of *Notch2* and *Sox9* are inter-correlated. *Sox9* overexpression in mice livers leads to increased *Notch2* expression levels through direct transcriptional activation [33]. Consequently, *Notch2* downregulation decreases *Sox9* expression, which minimises the growth that results from *Hnf4α* downregulation. However, *as* variant 3 tends to downregulate *Hnf4α* more than *Notch2*, it would be expected that *Sox9* expression would dramatically rise following variant 3 transfection. Similarly, it was anticipated that the levels of *Sox9* would drop after transfecting hepatoblasts with variant 7, which preferentially downregulates *Notch2* more than Hnf4α. These two traits were not readily apparent in the results. Therefore, there is no linear correlation between *Sox9* levels and *Hnf4α* /*Notch2* downregulation.

Conclusion

To conclude, this study optimised the isolation of liver progenitor cells. It established that 48h represents the optimal time for *miR-34a*-lipo transfection and activity. In addition, cells were able to start the hepatic specification process after 72 hours of *miR-34a* transfection. Moreover, the 5'-PHOS and PS at each end are the optimum chemical modifications for *miR-34a* activity and survival in the isolated hepatoblasts. After 48 hours, the variants showed selectivity between the two target genes. As such, variant 7 preferentially downregulated more *Notch2* while variant 3 downregulated more *Hnf4α*. Additionally, there was no clear relationship between *Sox9* expression and *Notch2* and *Hnf4α* downregulation following *miR-34a* transfection. As a result, these findings serve as a springboard for nucleic acid treatments that are more effectively delivered and more precisely targeted, particularly for liver disease and development.

References

1. Gordillo, M., Evans, T. & Gouon-Evans, V. Orchestrating liver development. *Development (Cambridge)* **142**, 2094–2108 (2015).
2. Yang, L. *et al.* The contributions of mesoderm-derived cells in liver development. *Semin Cell Dev Biol* **92**, 63–76 (2019).
3. Bort, R., Signore, M., Tremblay, K., Martinez Barbera, J. P. & Zaret, K. S. Hex homeobox gene controls the transition of the endoderm to a pseudostratified, cell emergent

epithelium for liver bud development. *Dev Biol* **290**, 44–56 (2006).
4. Zorn, A. M. Liver development. in (2008). doi:10.3824/stembook.1.25.1.
5. Ober, E. A. & Lemaigre, F. P. Development of the liver: Insights into organ and tissue morphogenesis. *J Hepatol* **68**, 1049–1062 (2018).
6. Si-Tayeb, K., Lemaigre, F. P. & Duncan, S. A. Organogenesis and Development of the Liver. *Dev Cell* **18**, 175–189 (2010).
7. Yang, L. *et al.* A single-cell transcriptomic analysis reveals precise pathways and regulatory mechanisms underlying hepatoblast differentiation. *Hepatology* **66**, 1387–1401 (2017).
8. Banales, J. M. *et al.* Cholangiocyte pathobiology. *Nat Rev Gastroenterol Hepatol* **16**, 269–281 (2019).
9. Antoniou, A. *et al.* Intrahepatic Bile Ducts Develop According to a New Mode of Tubulogenesis Regulated by the Transcription Factor *SOX9*. *Gastroenterology* **136**, 2325–2333 (2009).
10. Saliminejad, K., Khorram Khorshid, H. R., Soleymani Fard, S. & Ghaffari, S. H. An overview of microRNAs: Biology, functions, therapeutics, and analysis methods. *J Cell Physiol* **234**, 5451–5465 (2019).
11. Stucki, M. *et al.* Structure of Human DROSHA. *Cell* **164**, 81–90 (2016).
12. Annese, T., Tamma, R., de Giorgis, M. & Ribatti, D. microRNAs Biogenesis, Functions and Role in Tumor Angiogenesis. *Front Oncol* **10**, 1–21 (2020).
13. Nguyen, T. A., Park, J., Dang, T. L., Choi, Y.-G. & Kim, V. N. Microprocessor depends on hemin to recognize the apical loop of primary microRNA. *Nucleic Acids Res* **46**, 5726–5736 (2018).
14. Lund, E., Güttinger, S., Calado, A., Dahlberg, J. E. & Kutay, U. Nuclear Export of MicroRNA Precursors. *Science (1979)* **303**, 95–98 (2004).
15. Miller, S., Jones, L. E., Giovannitti, K., Piper, D. & Serra, M. J. Thermodynamic analysis of 5′ and 3′ single- and 3′ double-nucleotide overhangs neighboring wobble terminal base pairs. *Nucleic Acids Res* **36**, 5652–5659 (2008).
16. Liu, J. *et al.* Argonaute2 is the catalytic engine of mammalian RNAi. *Science* **305**, 1437–1441 (2004).
17. Bartel, D. P. Metazoan MicroRNAs. *Cell* **173**, 20–51 (2018).
18. Kaller, M. *et al.* Genome-wide characterization of *miR-34a* induced changes in protein and mRNA expression by a combined pulsed SILAC and microarray analysis. *Molecular and Cellular Proteomics* **10**, (2011).
19. Plata, C. A., Marni, S., Suweis, S., Bellini, T. & Paraboschi, E. M. Needles in Haystacks: Understanding the Success of Selective Pairing of Nucleic Acids. *Int J Mol Sci* **23**, (2022).
20. Tanimizu, N. & Miyajima, A. Notch signaling controls hepatoblast differentiation by altering the expression of liver-enriched transcription factors. *Journal of Cell Science* vol. 117 3165–3174 Preprint at https://doi.org/10.1242/jcs.01169 (2004).
21. Geisler, F. *et al.* Liver-specific inactivation of *Notch2*, but not Notch1, compromises intrahepatic bile duct development in mice. *Hepatology* **48**, 607–616 (2008).
22. Gilbert, M. A. *et al.* Alagille syndrome mutation update: Comprehensive overview of JAG1 and *NOTCH2* mutation frequencies and insight into missense variant classification. *Hum Mutat* **40**, 2197–2220 (2019).
23. Xiu, M.-X. & Liu, Y.-M. *The role of oncogenic Notch2 signaling in cancer: a novel therapeutic target*. *Am J Cancer Res* vol. 9 www.ajcr.us/ (2019).
24. Parviz, F. *et al.* Hepatocyte nuclear factor 4α controls the development of a hepatic epithelium and liver morphogenesis. *Nat Genet* **34**, 292–296 (2003).
25. Hsu, S. hao *et al.* Cationic lipid nanoparticles for therapeutic delivery of siRNA and miRNA to murine liver tumor. *Nanomedicine* **9**, 1169–1180 (2013).
26. Zatsepin, T. S., Kotelevtsev, Y. v. & Koteliansky, V. Lipid nanoparticles for targeted siRNA delivery - Going from bench to bedside. *Int J Nanomedicine* **11**, 3077–3086 (2016).
27. Kularatne, R. N., Crist, R. M. & Stern, S. T. The Future of Tissue-Targeted Lipid Nanoparticle-Mediated Nucleic Acid Delivery. *Pharmaceuticals* vol. 15 Preprint at https://doi.org/10.3390/ph15070897 (2022).
28. Semple, S. C. *et al.* Rational design of cationic lipids for siRNA delivery. *Nat Biotechnol* **28**, 172–176 (2010).
29. Desai, A. S., Hunter, M. R. & Kapustin, A. N. Using macropinocytosis for intracellular delivery of therapeutic nucleic acids to tumour cells. *Philosophical Transactions of the Royal Society B: Biological Sciences* **374**, (2019).
30. Tanimizu, N., Nishikawa, M., Saito, H., Tsujimura, T. & Miyajima, A. Isolation of hepatoblasts based on the expression of Dlk/Pref-1. *J Cell Sci* **116**, 1775–1786 (2003).
31. Smirnova, V. V *et al.* Ribosomal leaky scanning through a translated uORF requires eIF4G2. *Nucleic Acids Res* **50**, 1111–1117 (2022).
32. Joshua M Boucher, A. H. B. R. V. L. L. L. A receptor-specific function for *Notch2* in mediating vascular smooth muscle cell growth arrest through cyclin-dependent kinase inhibitor 1B. *Circ Res* **113**, 975–85 (2013).
33. Adams, J. M. *et al.* *Sox9* Is a Modifier of the Liver Disease Severity in a Mouse Model of Alagille Syndrome. *Hepatology* **71**, 1331–1349 (2020).
34. Freier, S. M. & Altmann, K. H. The ups and downs of nucleic acid duplex stability: structure-stability studies on chemically-modified DNA:RNA duplexes. *Nucleic Acids Res* **25**, 4429–4443 (1997).
35. Davis, S., Lollo, B., Freier, S. & Esau, C. Improved targeting of miRNA with antisense oligonucleotides. *Nucleic Acids Res* **34**, 2294–2304 (2006).
36. Xu, Y. *et al.* A metabolic stress-inducible *miR-34a*-HNF4α pathway regulates lipid and lipoprotein metabolism. *Nat Commun* **6**, (2015).
37. Salzman, D. W. *et al.* miR-34 activity is modulated through 5′-end phosphorylation in response to DNA damage. *Nat Commun* **7**, 10954 (2016).
38. Basyuk, E., Suavet, F., Doglio, A., Bordonné, R. & Bertrand, E. Human let-7 stem–loop precursors harbor features of RNase III cleavage products. *Nucleic Acids Res* **31**, 6593–6597 (2003).
39. Marzi, M. J. *et al. Degradation dynamics of microRNAs revealed by a novel pulse-chase approach Running Title: Uncovering miRNA decay in mammalian cells by metabolic labeling*.
40. Haraszti, R. A. *et al.* 5′-Vinylphosphonate improves tissue accumulation and efficacy of conjugated siRNAs in vivo. *Nucleic Acids Res* **45**, 7581–7592 (2017).
41. Elkayam, E. *et al.* siRNA carrying an (E)-vinylphosphonate moiety at the 5′ end of the guide strand augments gene silencing by enhanced binding to human Argonaute-2. *Nucleic Acids Res* **45**, 3528–3536 (2017).
42. Haraszti, R. A. *et al.* 5′-Vinylphosphonate improves tissue accumulation and efficacy of conjugated siRNAs in vivo. *Nucleic Acids Res* **45**, 7581–7592 (2017).
43. Riolo, G., Cantara, S., Marzocchi, C. & Ricci, C. miRNA targets: From prediction tools to experimental validation. *Methods and Protocols* vol. 4 1–20 Preprint at https://doi.org/10.3390/mps4010001 (2021).
44. Elkayam, E. *et al.* SiRNA carrying an (E)-vinylphosphonate moiety at the 5′ end of the guide strand augments gene silencing by enhanced binding to human Argonaute-2. *Nucleic Acids Res* **45**, 3528–3536 (2017).
45. Prakash, T. P. *et al.* Identification of metabolically stable 5′-phosphate analogs that support single-stranded siRNA activity. *Nucleic Acids Res* **43**, 2993–3011 (2015).
46. Liang, C. A. L. C. Sulfur does not form double bonds in phosphorothioate anions. *J Am Chem Soc* **109**, 6449–6453 (1987).